Understanding Activity-Stability Tradeoffs in Biocatalysts by Enzyme Proximity Sequencing

Rosario Vanella[1, 2, *], Christoph Küng[1, 2], Alexandre A. Schoepfer[1], Vanni Doffini[1,2], Jin Ren[1,2], Michael A. Nash[1, 2, 3, 4 *]

[1] Institute of Physical Chemistry, Department of Chemistry, University of Basel, 4058 Basel, Switzerland
[2] Department of Biosystems Science and Engineering, ETH Zurich, 4058 Basel, Switzerland
[3] National Center for Competence in Research (NCCR), Molecular Systems Engineering, 4058 Basel, Switzerland
[4] Swiss Nanoscience Institute, 4056 Basel, Switzerland
* Correspondence to: rosario.vanella@unibas.ch; michael.nash@unibas.ch

Abstract

Understanding the complex relationships between enzyme sequence, folding stability and catalytic activity is crucial for applications in industry and biomedicine. However, current enzyme assay technologies are limited by an inability to simultaneously resolve both stability and activity phenotypes and to couple these to gene sequences at large scale. Here we developed Enzyme Proximity Sequencing (EP-Seq), a deep mutational scanning method that leverages peroxidase-mediated radical labeling with single cell fidelity to dissect the effects of thousands of mutations on stability and catalytic activity of oxidoreductase enzymes in a single experiment. We used EP-Seq to analyze how 6,387 missense mutations influence folding stability and catalytic activity in a D-amino acid oxidase (DAOx) from *R. gracilis*. The resulting datasets demonstrate activity-based constraints that limit folding stability during natural evolution, and identify hotspots distant from the active site as candidates for mutations that improve catalytic activity without sacrificing stability. EP-Seq can be extended to other enzyme classes and provides valuable insights into biophysical principles governing enzyme structure and function.

Introduction

Soluble proteins produced through natural selection are typically only marginally stable. For enzymes, local flexibility is required at the active site to achieve catalytic activity, however excessive mobility renders them susceptible to denaturation. This tradeoff between activity and stability is still not well understood in protein science[1–3]. Observations on small numbers of homologous sequences have shown how cold-adapted enzymes are typically more active than thermophilic homologs[4–6], however, competing studies relying on database meta-analysis[7], experimental data and comparative phylogenetics[8] have challenged this thermal rate compensation model. The question of how enzymes encode activity and stability, and the interplay between the two over the course of natural evolution or during experimental laboratory directed evolution[9,10] therefore remains open. For enzyme engineering, these trade offs mean that both stability and activity cannot be optimized simultaneously or with equal success. If we could experimentally determine sequence-function relationships describing folding stability and catalytic activity of enzyme variants at large scale, it would enable an understanding of the activity-stability tradeoff, and potentially unlock enhanced enzymes for industrial and biomedical applications.

With the advent of deep mutational scanning (DMS), the effects of large numbers of genetic mutations on protein phenotype can be analyzed using massively parallel methods[11–13]. However, catalytic enzymes are challenging for DMS studies because there exist very few massively scalable screening methods which successfully link genotype and phenotype. Typically, enzyme fitness is coupled to host cell survival using growth-based selection. Alternatively, microdroplet methods allow single clones to be analyzed using colorimetric assays followed by droplet sorting and sequencing. Enrichment of variants from pre- to post-selected pools allows tabulation of phenotypic scores and provides insights into mutational fitness landscapes[14–20]. In nearly all prior implementations of DMS on enzymes, however, fitness scores comprise a conflation of expression level (i.e. enzyme abundance) and catalytic activity. Klesmith and colleagues showed how enzyme fitness scores determined through growth-based selection could be combined with solubility scores from independent assays to reveal evolutionary origins of stability activity trade-offs[21]. Markin *et al.* further presented a microfluidic enzyme expression platform which decoupled the catalytic properties of each variant from their expression levels[22]. While very powerful, each platform has associated limitations in terms of throughput, ease-of-use, compatible chemistries, and robustness.

Here we report EP-Seq, a novel DMS-based method that combines enzyme proximity labeling with next-generation DNA sequencing (NGS) technology to assay both expression level and catalytic activity phenotypes of thousands of variant enzymes from a cellular pool in a single experiment. EP-Seq leverages features of yeast surface display[23,24] to measure the expression levels of each enzyme variant *via* a pooled cell sorting-sequencing experiment. In parallel, phenoxyl radical-based[25–27] cell surface proximity labeling links enzyme activity to a fluorescent signal, which is then quantified by sorting and sequencing. We used EP-Seq to study a nearly comprehensive site saturation mutational library of D-amino acid oxidase from the yeast *Rhodotorula gracilis*, a model flavoprotein with industrial and therapeutic applications[28–33]. Downstream computational analysis of EP-Seq data reveals rich biophysical insights into the enzyme by quantifying fitness propensities of substituted residues, identifying protein regions where catalytic activity served as an evolutionary constraint on

folding stability, and making predictions of catalysis-enhancing mutations that maintain folding stability.

Results and discussion

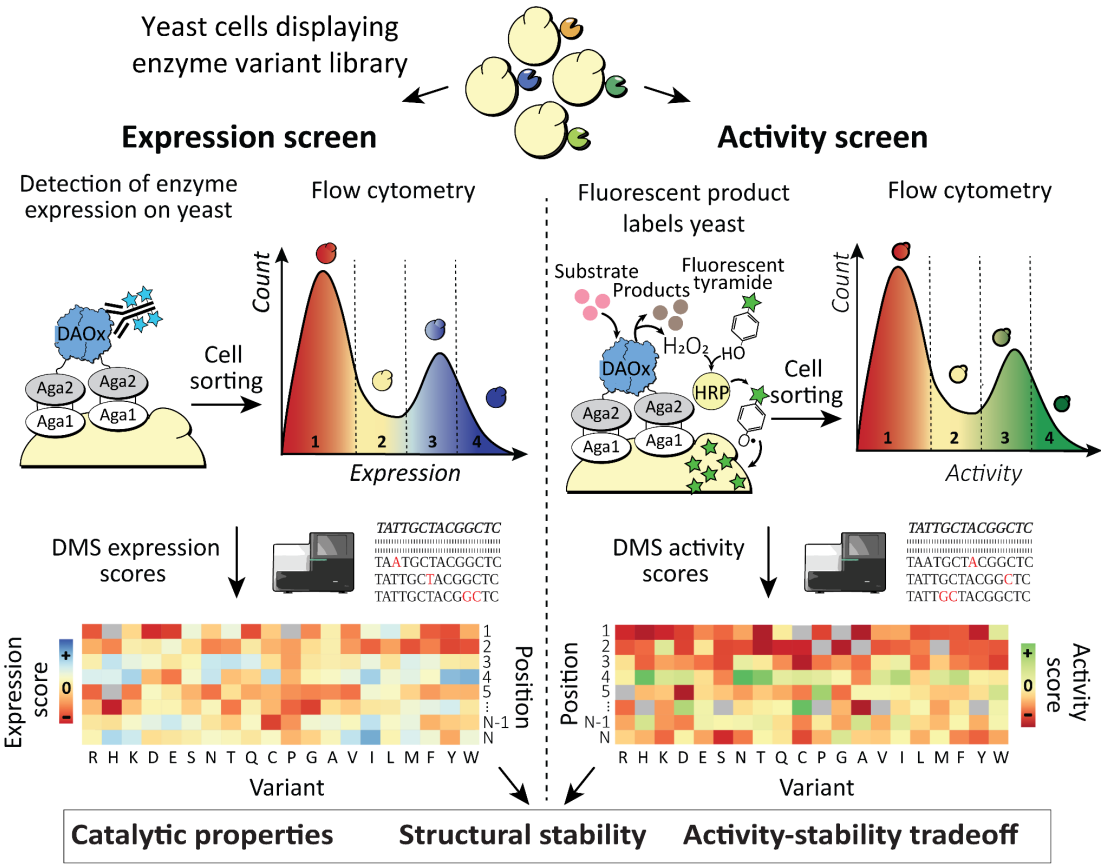

Figure 1. Schematic depicting the EP-Seq workflow. (Top) A pooled library of enzyme variants is displayed on yeast. (Left) The cell population is sorted into bins based on the expression level of the displayed enzyme. (Right) The pooled variant library is assayed for DAOx activity using a cascade peroxidase-mediated proximity labeling reaction with single cell fidelity and sorted into bins. The genetic composition of cells in the sorted bins is quantified via high-throughput sequencing and the distribution of each variant along the expression and activity axes is converted into a fitness score. Joint analysis of the two independent datasets provides insights into the effects of mutations on structural stability and activity of the enzyme.

Workflow overview.

An overview of the EP-Seq workflow is shown in Figure 1. In one branch of the experiment (Fig. 1, left), we analyze the expression levels of thousands of variants in parallel by displaying a variant library on yeast, staining the expressed proteins with fluorescent antibodies, and sorting the cells into 4 bins using fluorescence activated cell sorting (FACS). We then use NGS to sequence the variants in each bin, and convert the NGS reads into expression fitness scores using a custom computational pipeline. There is strong evidence that the level at which yeasts secrete and display a given protein sequence is correlated with its folding stability[21,24]. Destabilizing mutations can activate the yeast quality control system, exposing variants to proteases in the secretory pathway which degrade unstable sequences

and lower expression levels[34]. The expression level of a variant enzyme analyzed through FACS and DMS can therefore serve as a proxy for folding stability.

In a parallel branch of the experiment (Fig. 1, right), the oxidase activity of enzyme variants is assayed at large scale in a pooled format using a horseradish peroxidase (HRP)-mediated phenoxyl radical coupling reaction at the yeast surface. Similar proximity labeling reaction schemes relying on HRP or ascorbate peroxidase-2 (APEX2) have been used in quantitative proteomics[35], proximity labeling in live cells[36–39], electron microscopy labelling[40,41] and signal amplification in biosensors[42,43]. In EP-Seq, the short half-life of phenoxyl radicals limits the labeling reaction to the surface of the cell that generates H_2O_2, affording an artificial quasi single-cell reaction compartment by means of a reaction-diffusion limitation. The pooled cells displaying the variant library stained in this fashion are sorted into bins based on fluorescent intensity, and sequenced by NGS. Finally, the large datasets obtained in the two parallel screening protocols are combined, cross-referenced and studied to reveal biophysical insights into protein sequence, stability, and function.

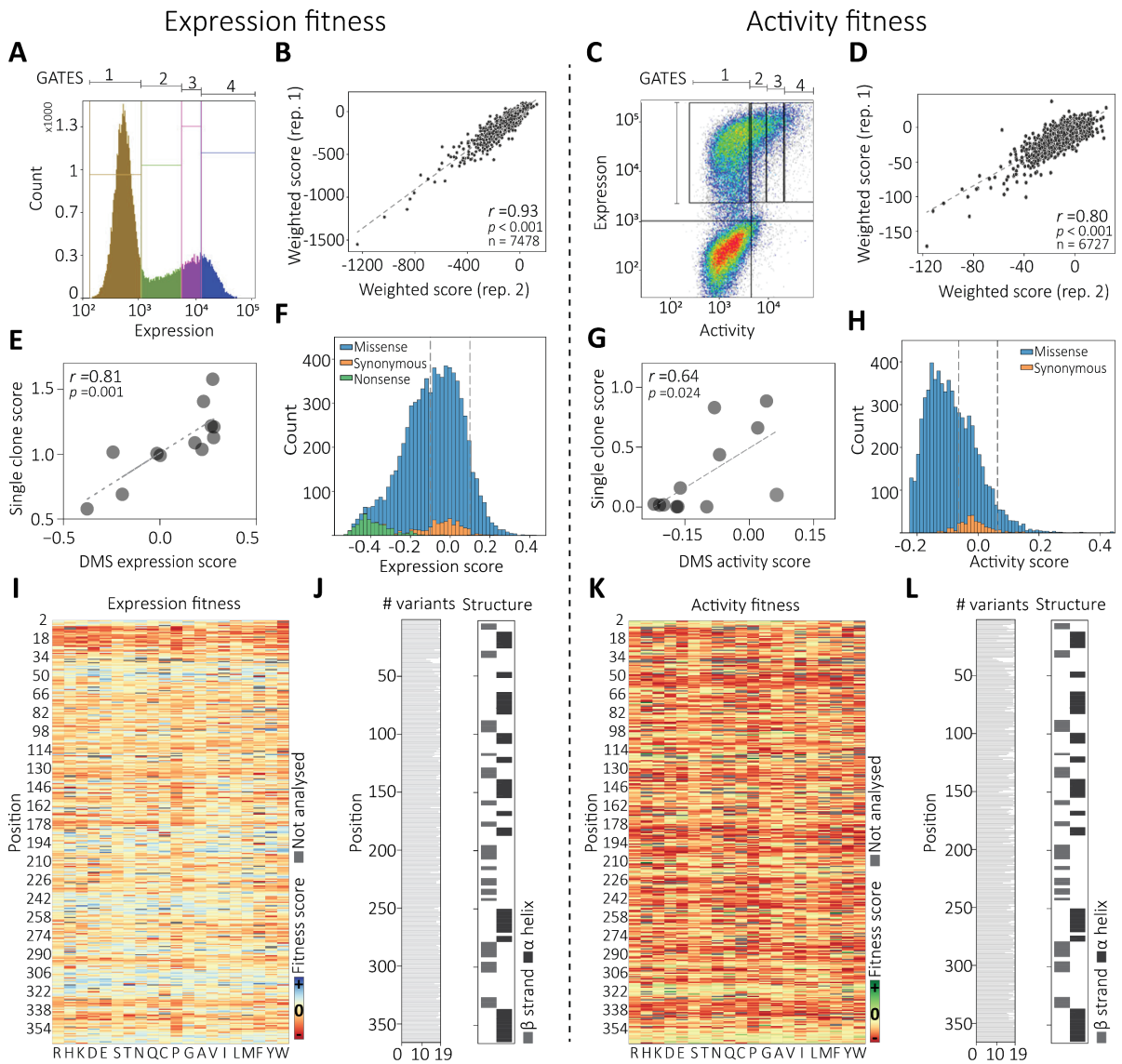

Figure 2. Deep mutational scanning of DAOx expression and catalytic activity by EP-Seq. A) Sorting gates for analysis of display levels. B) Linear correlation between weighted expression fitness calculated from two biological replicates. C) Sorting gates for catalytic activity screening. D) Linear correlation between weighted activity fitness calculated from two biological replicates. E) Correlation between variant surface display level measured in monogenic yeast culture vs. DMS expression fitness analyzed by EP-Seq for 12 DAOx single mutant variants. F) Distribution of expression fitness effects measured by EP-Seq. G) Correlation between variant activity level measured in monogenic yeast culture via peroxidase assay (AmplexRed) vs. DMS activity fitness analyzed by EP-Seq for 12 DAOx single mutant variants. H) Distribution of activity fitness effects measured by EP-Seq. I) Expression fitness scores for each variant represented as a heatmap. J) Number of variants analyzed per position in the expression dataset, and secondary structure classification per position (PDB 1C0P). K) Activity fitness scores for each variant obtained by EP-Seq represented as a heatmap. L) Number of variants analyzed per position in the activity dataset and secondary structure classification per position (PDB 1C0P).

Quantifying DAOx stability and catalytic activity fitness with EP-Seq scores.

We applied the workflow described above to study the 80 kDa homodimeric flavin adenine dinucleotide (FAD) dependent DAOx from *Rhodotorula gracilis* (*Rg*), which promiscuously catalyzes deamination of D-amino acids to imino acids, generating H_2O_2 as a byproduct[33]. DAOx has attracted attention for applications in both industry and biomedicine, for example, in resolving racemic amino acid mixtures, producing antibiotics[30] or as a proposed cancer therapy via reactive oxygen species[28,29,44]. We first optimized the functional expression and display of the wild type DAOx (WT

DAOx) fused with the Aga2 anchor protein and established the tyramide-based proximity labeling assay to detect the activity of each displayed enzyme with single-cell fidelity (Supplementary Note 1). Next, we constructed a library for DMS analysis through site saturation mutagenesis over the entire coding region of DAOx and assigned 15 nucleotides unique molecular identifier (UMIs) to each DAOx variant of the library (Supplementary Note 2).

We investigated the effects of single amino acid substitutions on DAOx expression and display at the yeast surface (Fig. 2, left). Following induction (48 h, 20°C at pH 7), we stained the C-terminal His-tag of the DAOx variant library with primary and fluorescent secondary antibodies. We sorted the library into 4 bins based on expression level, where the non-expressing bin was set using a negative control cell population incubated with only the secondary antibody. The remaining yeasts were sorted into three sub-populations containing equal percentages of expressing cells (Fig. 2*A*). After sorting, we extracted plasmid DNA from each sorted cell population, PCR amplified the regions corresponding to the UMIs, and sent the amplicons for single end (SE100) Illumina sequencing on a NovaSeq 6000. The number of reads per sample was on average 4-fold higher than the number of cells sorted into the corresponding FACS bin (Table S2). We filtered the UMI sequences by read quality (Phred score > Q20) and expected size (15 nucleotides) before assigning them to the corresponding DAOx variants using the look-up table. We converted the number of reads per variant into number of cells (Methods, Equation 1) and calculated a final expression score (Exp) for each variant (Methods, Equation 2). The fitness score per variant was then calculated as $\log_2(\beta_v/\beta_{wt})$ where β_v was the weighted mean expression score of the variant enzyme and β_{wt} was the score of WT DAOx .

To analyze DAOx catalytic activity in a massively parallel fashion, we used a reaction cascade that converts DAOx enzymatic activity into a fluorescent label on the cell wall. This approach is related to prior work from our lab and others on enzyme-mediated polymerization and peroxidase-based proximity labeling[13,26,27,45,46]. We set the low fluorescence gate to include entirely the population of cells displaying inactive variants (Fig. 2*C*, Gate 1). The remaining cells were equally divided into three populations corresponding to increasing levels of tyramide-488 signal (Fig. 2*C*). We determined the genetic sequences and their relative abundance in each bin through Illumina sequencing as described above, and identified the corresponding mutant enzyme sequences using the look-up table. The activity score (Act) per variant was calculated using a weighted approach (Methods, Equation 3) and the activity fitness score was computed by using as reference the score of the wild type DAOx.

In both the expression and activity screens, we determined a consensus score for each mutant by calculating a weighted mean fitness using the number of cells for each variant in the two replicates as the weight (Methods, Equation 4). This allowed us to place more emphasis on fitness values that were represented by a higher number of cells in an experimental replicate, resulting in final consensus fitness scores that were calculated with higher confidence. We assessed the reproducibility of the DMS workflow by calculating Pearson's *r* value for a linear regression of the weighted fitness scores measured in two biological replicates. For the expression assay replicates, the *r* value was 0.93 (n=7,478; $p<0.001$), and for the activity assay replicates, it was 0.80 (n=6,727; $p<0.001$)(Fig. 2*B, D*).

Validation of EP-Seq scores.

To validate the DMS fitness scores of single clones, we randomly selected 12 variants and tested them individually using bulk expression and activity assays. The expression levels of the variants measured

individually using yeast display and flow cytometry strongly correlated with expression fitness scores obtained from DMS (r=0.81, p=0.001) (Fig. 2*E*). The activity levels of the same 12 single mutant variants were next measured using an Amplex red assay, and the initial reaction rate was measured for the mutants and the wild type enzymes. The single clone score for each mutant was obtained by dividing initial reaction rate of the mutant by that of wild type. 10 out of 12 mutants (>80%) showed activity levels consistent with those obtained from EP-Seq (r=0.64, p=0.024) (Fig. 2*G*). We note that codon differences may contribute to slight discrepancies in comparative measurements with single-clones because our DMS scores correspond to an average score for synonymous codons.

To further validate the observed scores, we plotted a histogram to visualize the expression (Fig. 2*F*) and activity (Fig. 2*H*) fitness scores of all single nucleotide variants in the DAOx gene and color coded them to distinguish between missense, nonsense (i.e. Stop codon), and synonymous mutations. We found the distribution of missense mutational scores for both expression (n=6,769 variants) and activity (n=6,396 variants) fitness were broadly distributed. The distribution of expression scores for missense variants was also highly symmetric (Fig. 2*F*). Fitness score distributions were on average offset towards negative fitness values, indicating a generally deleterious effect of mutation on both expression and activity (median Exp = -0.07, median Act = -0.1**,** Fig. 2*F,H*). The distribution of fitness scores containing synonymous mutations in the expression screen was centered at -0.03 ± 0.091 (n=349 variants), while in the activity screen it was centered at -0.01 ± 0.064 (n=331 variants). This range of fitness values defined a neutral fitness range of the assay. Variants who's scores fell in this range were expected to have fitness comparable to that of WT. Additionally, mutants with nonsense mutations (i.e. stop codons) had strong negative fitness, with average score of -0.37 ± 0.1 (n=360) (Fig. 2*F*). Nonsense mutations could not be analyzed for the activity screen because the 2D FACS sorting strategy removed variants lacking the C-terminal His-tag from the sequenced pools (Fig. 2*C*).

As further validation, we calculated the average expression and activity scores per position (n=364) and mapped the values onto the DAOx structure (PDB 1C0P) (Fig. S4, A,B). We tested for EP-Seq score correlation with a protein stability prediction algorithm (FOLDX)[47] (Methods, Equation 5). We used FOLDX to calculate the mean ΔΔG score per position of the protein (n=360) and compared them to expression fitness scores obtained from the left branch of EP-Seq. We found strong correlations between EP-Seq expression scores and predicted ΔΔG values (Exp rho=-0.49 p<0.001, Fig. S4*C*), supporting the use of yeast surface display for evaluating the effects of mutations on thermodynamic folding stability. We further compared the predicted ΔΔG values to EP-Seq catalytic activity scores per position of DAOx and again found significant correlation (Act rho=-0.49 p< 0.001, Fig. S4*D*). This result supports the idea that a baseline level of structural stability is required for an enzyme to be catalytically active, and that at least part of the EP-Seq activity score is attributable to effects of mutations on the structural stability (and therefore expression) of DAOx.

Mutability landscapes of DAOx stability and catalytic activity.

We visualized the mutational effects of the 6,769 and 6,396 missense mutations in the expression and activity screens (respectively) as fitness heatmaps (Figures 2 I,K). These numbers corresponded to 97.9% and 92.4% (respectively) of all possible single amino acid substitutions in DAOx (Fig. 2J,L). The expression heatmap (Fig. 2*I*) reveals patterns of higher and lower tolerance for mutation along the DAOx sequence, discussed in detail below. Noteworthy was an N-terminal region (residues 8-32) found to be highly intolerant to amino acid substitutions. This suggests it plays a role in folding stability

and could act as an N-terminal intra-molecular chaperone[48]. The Rossmann fold is highly conserved in this region, making contact with the FAD cofactor, stabilizing structure and maintaining function of the enzyme[33].

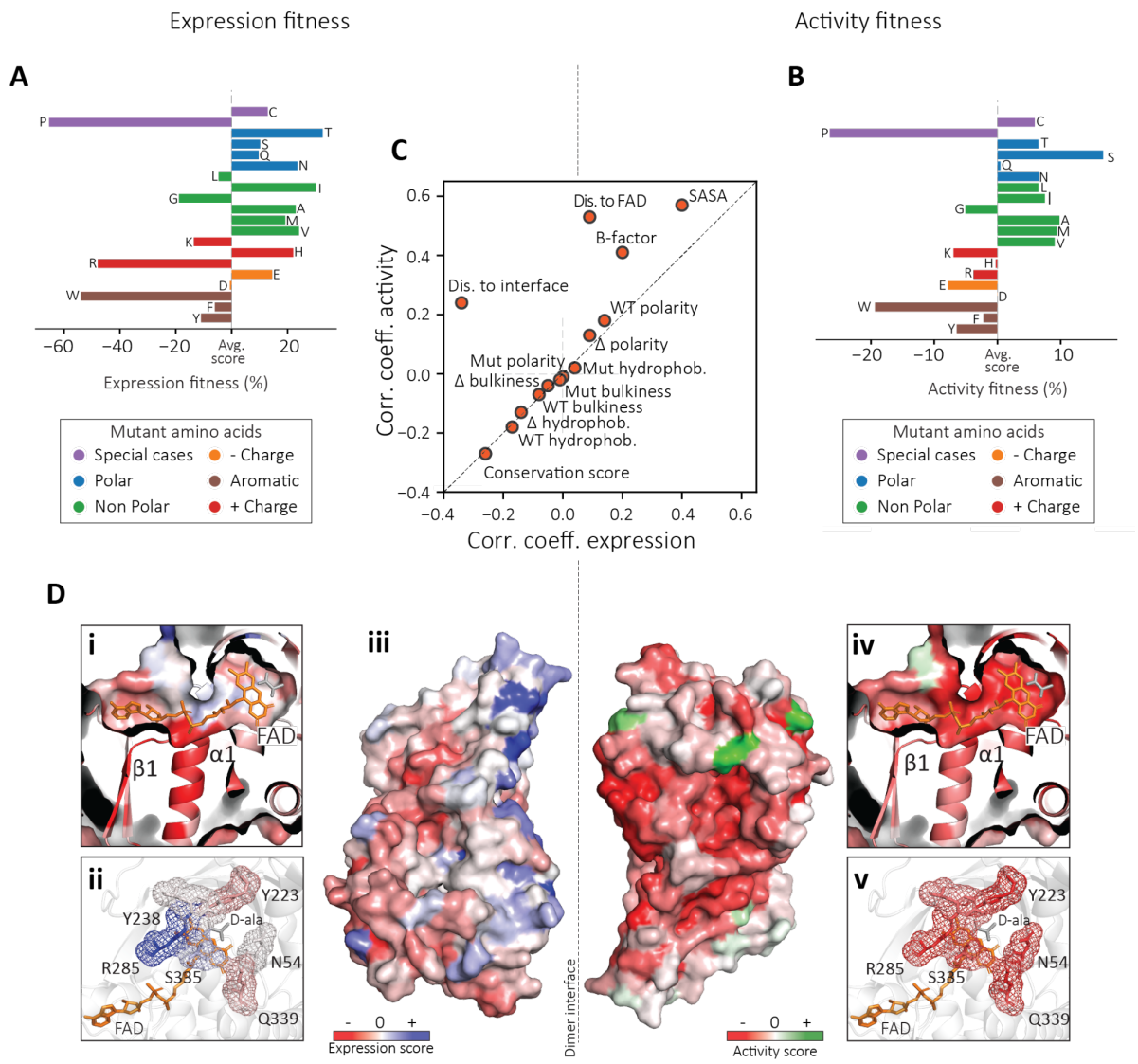

Figure 3. EP-Seq reveals biophysical properties that differentially influence expression and activity. A) Relative impact of mutant residue identity on DAOx expression. B) Relative impact of mutant residue identity on the DAOx enzymatic activity. C) Plot of Pearson correlation coefficients (*r*) calculated for expression (x-axis) or activity (y-axis) fitness scores with respect to several biophysical properties of mutated sites in DAOx. D) DAOx structure colored by expression or fitness scores: (i) Residues surrounding FAD cofactor colored by expression score; (ii) Residues contacting the substrate D-alanine colored by expression score; (iii) Expression (left) or activity (right) scores used to color the surface of DAOx monomers. The monomers are shown separated from each other to improve visibility of the interface; (iv) Residues surrounding FAD cofactor colored by activity score; (v) Residues contacting the substrate D-alanine colored by activity score.

Thermodynamic stability shapes both expression and activity landscapes.

We evaluated the effect of mutant residue identity on both expression and activity of DAOx using data from 6,387 single missense variants for which both EP-Seq expression and activity scores were available (Fig. 3A, B, Table S4, Supplementary Note 3). We observed that the introduction of proline

had the most pronounced negative impact on both expression and activity, particularly when located in the α helix and β sheet regions of DAOx (Fig. S5*A,B*, Supplementary Note 4). The introduction of cysteine, neutral polar and non-polar residues (excluding glycine and leucine) had a positive impact on the studied properties, while the introduction of charged residues (excluding histidine and glutamic acid) resulted in a lower fitness score than average. Finally, among hydrophobic residues, introduction of bulky tryptophan impaired both expression and activity fitness (Fig. 3*A* , Table S4). As a general trend we also observed that DAOx linker regions had greater tolerance to mutations in both expression and activity screens compared to structured regions of the same enzyme (Fig. S5*C,D*, Supplementary Note 4). We next analyzed expression and activity fitness as a function of the substituted wild type amino acids (Fig. S5*E,F*, Supplementary Note 5) and found the substitution of hydrophobic core aromatic residues together with valine, which is one of the most abundant residues in DAOx (n=27), to have the highest negative impact on the expression and activity of the enzyme. On the contrary, mutation of polar and charged amino acids was associated with on average higher scores than the other classes of residues (Fig. S5*E,F*, Supplementary Note 5).

Next, we assigned residue specific scores for hydrophobicity, bulkiness and polarity of wild type and mutant amino acids [49] to each of the 6,387 single missense mutations registered by both assays and calculated a Pearson linear correlation coefficient *r* between the values of each feature and the experimental fitness scores (Fig. 3*C*, Fig. S6*A*). We observed no or very low linear correlation between the experimental scores and properties of mutant residues (Mut. hydrophobicity, Mut. polarity, Mut. bulkiness, Fig. S6*A*). Consistent with our previous observations, the hydrophobicity of wild type residues negatively correlated with both expression (r=-0.17, p<0.001) and activity scores (r=-0.18, p<0.001), suggesting low tolerance for mutations in the protein core (WT, Δ hydrophobicity, Fig. 3*C*, Fig. S6*A*). We found moderate negative correlation of both expression and activity datasets when considering the size of wild type amino acids or the size difference between wild type and mutant residue side chains (Fig. 3*C*, Fig. S6*A*, WT and Δ bulkiness). Finally, a positive correlation of expression (r=0.14, p<0.001) and activity scores (r=0.18, p<0.001) with the polarity of wild type amino acids indicated higher tolerance for mutation of polar residues, typically found on the surface of the protein (Fig. 3*C*, Fig. S6*A*, WT and Δ polarity).

Stability activity trade-offs along natural evolution of DAOx.

We next sought to determine whether our expression and activity datasets could be used to identify regions of stability-activity tradeoffs. We analyzed average expression and activity scores of DAOx at each position (n_{Epx}=n_{Act}=360) in relation to biophysical properties of the mutated sites (Fig. 3*C*) and observed several trends. For example, both expression and activity fitness scores were positively correlated with solvent accessible surface area (SASA) of the mutated site (Expression: r=0.40, p<0.001; Activity: r=0.57, p<0.001). The temperature factor (B-factor) was similarly positively correlated with both fitness scores (Expression: r=0.2, p<0.001; Activity: r=0.41, p<0.001) indicating higher mutational tolerance at sites located at the protein surface and at sites with high structural mobility (Fig. 3*C*, Fig. S6*B,C*).

We analyzed fitness scores of mutated sites with respect to their distance from the FAD cofactor (Fig. 3*C*, Dis. to FAD). We found that mutations near FAD often negatively impacted the catalytic activity of the enzyme, as indicated by the positive correlation between the activity scores and the distance of the mutated residue from FAD (r=0.53, p<0.001, Fig. S6*D* bottom). In contrast, expression fitness

scores were not significantly correlated with distance of the mutated residue to FAD (r=0.09, p=0.086, Fig. S6*D* top), suggesting that structural stability was insensitive to this parameter. We color-coded the 3D structure of DAOx according to activity and expression scores in the vicinity of the FAD cofactor and in the active site (*Fig 3D i, ii, iv, v*), where we found the largest differences between the activity and expression scores. Mutations in close proximity to FAD (distance<4 Å) greatly impaired the catalytic activity of the enzyme (avg. Act=-0.125,-40%, avg. Act all=-0.089, Fig. 3*DIV*) while at the same positions the expression scores showed the opposite trend. This shows that mutations at the catalytic site tended to harm activity but improve stability (avg. Exp=-0.068, +12%, avg. Exp all=-0.077, Fig. 3*DI*), suggesting the enzyme pays a thermodynamic price to remain catalytically active under conditions of functional selection.

A similar behavior was found for residues known to coordinate the substrate D-alanine[33]. While mutating these residues impaired enzyme activity (avg. Act= -0.128, -44%, avg. Act all =-0.089, Fig. 3*DV*), it tended to improve stability (avg. Exp=-0.004, +95%, avg. Exp all= -0.077, Fig. 3*DII*). Among the residues interacting with FAD, the loop between strand β1 and helix α1 is highly conserved among Rossmann folds (GSGVIGL, positions: 11-17) and is characterized by negative fitness scores in both datasets (avg. Exp =-0.232 , avg. Act=-0.113) (Fig. 3*DI,IV*). This suggests both a functional and structural role of FAD in the overall fitness of the enzyme. These results suggest DAOx folding is facilitated by interactions with FAD, which is also essential for its catalytic activity. The strong binding affinity between DAOx and FAD (K_D=20 nM) and the low abundance of apo-enzyme further support these observations [50,51].

Dimerization stabilizes marginally stable but functional DAOx monomers.

DAOx is active as a homodimer in its native state and dimerization is thought to be required for activity[51,52]. This motivated a detailed analysis of mutations in close proximity to the dimer interface, and whether they could significantly change thermodynamic stability and catalytic activity of the enzyme. We calculated the distance between each residue and the closest residue found at the dimer interface, and assigned this distance value to each single missense mutation found in both the expression and activity screens. We then calculated a linear correlation coefficient between the experimental fitness scores and the distance values. We found that the activity fitness data showed a positive correlation with the distance of the mutated site from the dimer interface (r=0.24, p<0.001, Fig. 3*C*, Dis. to interface, Fig. S6*E* bottom), while the expression scores correlated negatively with it (r=-0.34, p<0.001, Fig. 3*C*, Dis. to interface, Fig. S6*E* top). On average, sites located closer to the dimer interface were more tolerant to mutation in the expression screen, but less so for the activity screen. This reflects a scenario where the enzyme tolerates some amount of instability in order to remain as an active dimer, analogous to the effects at the catalytic site. We visualized these effects on the surface of the 3D structure of the DAOx dimer (Fig. 3D iii). Mutations located at the dimer interface impaired the catalytic activity of the DAOx enzyme as indicated by the dominant red color of the structure (avg. Act=-0.093, -6%, avg. Act all=-0.088, Fig. 3D iii, right). The same mutations showed overall positive effects on the expression and stability of the DAOx structure (avg. Exp=-0.005, +93%, avg. Exp all=-0.076, Fig. 3Diii, left). We attributed this behavior to a strong dependency of DAOx catalytic activity on dimerization[51,52]. Apparently, dimerization along with the conformation of the catalytic site provide functional constraints during evolution of this enzyme, suggesting the evolution of a more stable globular and monomeric form of DAOx might have been impeded during functional selection for catalytic activity.

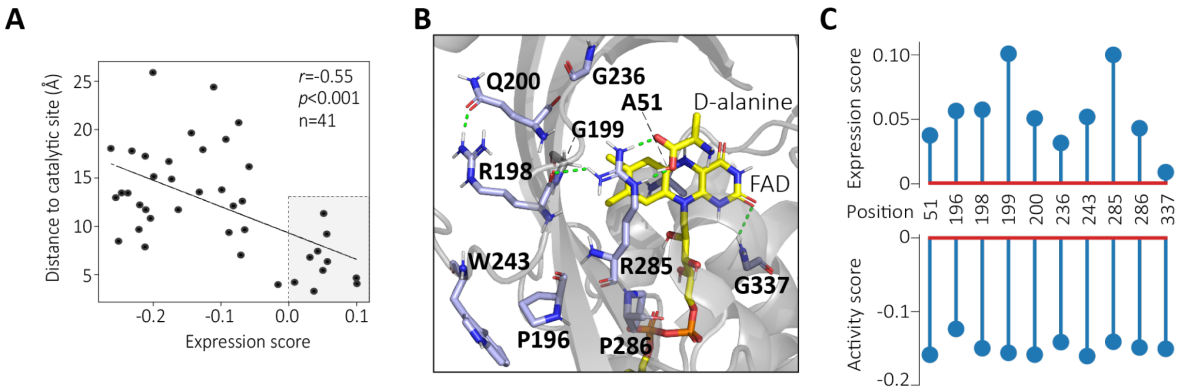

Figure 4. EP-Seq and sequence conservation analysis reveal functional sites of DAOx. A) The distance to the catalytic site for positions that are evolutionarily conserved (conservation score, CONS = 100) were analyzed as a function of EP-Seq expression scores (average per position). The ten highly conserved residues associated with the most positive expression scores (light gray box) are visualized in B. B) Structural details of DAOx residues with CONS = 100 and expression score > 0. H-bonds are shown in green. The FAD cofactor and D-Ala carbon backbones are colored in yellow. DAOx residue carbon backbones are colored in light blue with colored elements: Hydrogen (white), Nitrogen (dark blue), Oxygen (Red), Phosphorus (Orange). C) Expression and activity scores for each of the conserved positions linked to positive expression scores.

EP-Seq expression scores combined with sequence conservation reveal functional sites in DAOx. Sequence conservation scores derived from multisequence alignment reflect constraints imposed on the protein of interest as a result of natural selection. Over evolutionary time, selection tends to maintain both folding stability and catalytic activity[53,54]. We hypothesized that combining conservation scores with our stability and activity datasets could provide insights into functional sites in DAOx. We compared the experimental scores with conservation scores (CONS) obtained by aligning the DAOx sequence with five evolutionarily related D-amino acid oxidase sequences (Fig. S7). Both expression and activity fitness score datasets showed negative correlation with conservation scores (Exp r=-26, p<0.001; Act r=-27, p<0.001, Fig. 3*C*, Fig. S6*E*), generally indicating higher tolerance for mutations at less conserved protein sites. We identified 41 positions with CONS=100 and analyzed the average expression score per position as a function of the distance of the mutated site from the catalytic center of DAOx. We observed a significant negative correlation of the expression scores with the distance of the mutation from the catalytic site of the enzyme (r=-0.55, p<0.001, Fig. 4*A*). Among the sites with conservation score 100, we then isolated the positions associated with positive expression score (n=10) and visualized them on the 3D structure of DAOx (Fig. 4*B*). Four of the positions analyzed (A51, G199, R285, G337) are found within 5Å of the active site are reported to be directly involved in catalysis through stabilization of the substrate D-alanine (R285) or of the isoalloxazine ring of FAD cofactor (A51, G199, G337)[33]**.** Other conserved residues (R198, Q200, G336), including two prolines in position 196 and 286, are part of three antiparallel strands β8, β12 and β13 suggesting a role of the resulting β sheet in structuring the catalytic pocket and coordinating the side chain of the Arginine 285. Finally, tryptophan W243 located at the surface of monomeric DAOx plays an important role in the dimerization. In agreement with the previous observations, its mutation has a direct impact on the catalytic efficiency of the DAOx[55] (Fig. 4*B*).

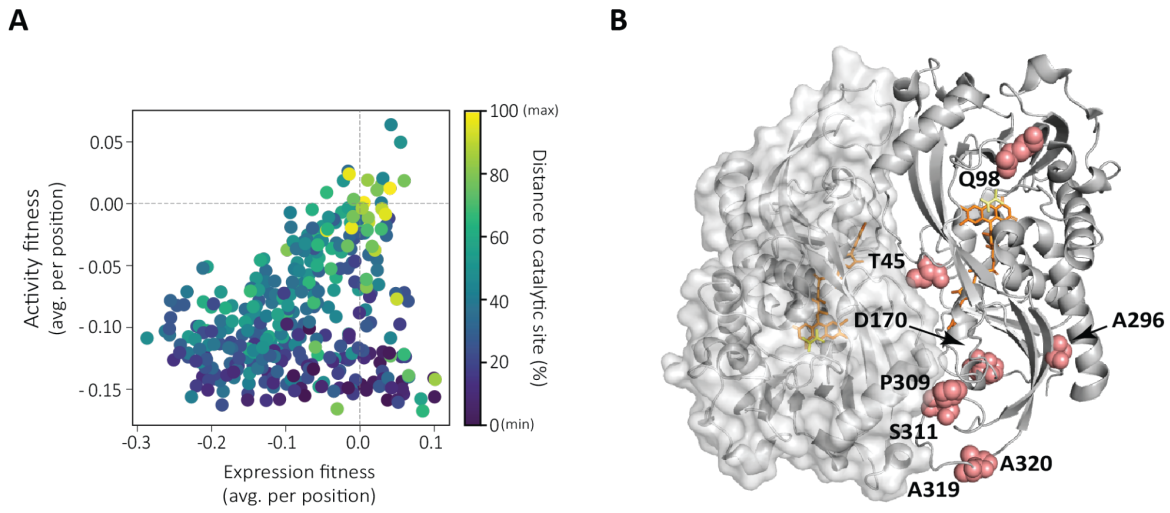

Figure 5. EP-Seq predicts activity enhancing mutations in DAOx. (A) Average expression and activity fitness scores per position in the DAOx enzyme. The coloring indicates distance to the active site. (B) Positional hotspots (spheres) where mutation on average increased DAOx activity. The FAD cofactor is visualized in orange and D-alanine in yellow.

Activity enhancing hotspots are globally encoded.

We next used EP-Seq to identify hotspots where mutation was associated with improved catalytic activity. We generated a two-dimensional scatterplot showing the average activity and expression fitness per position as Y and X coordinates (Fig. 5*A*), and assigned a color at each point based on the distance of the mutated site to the enzyme's catalytic pocket. The observed trends in this depiction demonstrate how the two properties are related. Variants that are found to be catalytically active must possess at least a minimum level of structural stability in order to be correctly folded, secreted and displayed. This fact is demonstrated by a lack of positions in the upper left of the plot. Only 5 positions (~1%) were found with positive activity fitness and negative expression fitness (Fig. 5*A*, top left)**.** Additionally, we found 33 positions (~9%) exhibiting positive expression fitness with significantly impaired catalytic activity (activity fitness <-0.1) (Fig. 5*A*, lower right). These positions tended on average to be closer to the catalytic site (avg. distance=12 Å; avg. distance all=17 Å), indicated by the dark blue color in the lower right of the plot. This demonstrates structure-function tradeoffs at play in this enzyme, where more stably expressed variants could be found by mutating crucial catalytic residues at the cost of losing activity. Finally, many mutations which moderately altered the expression of the enzyme resulted in corresponding changes in the catalytic activity (Fig. 5*A*, diagonal). A limited number of positions were tolerant to mutations for both assayed properties (n=10) (Exp>0; Act>0) and showed either simultaneous improvement of both properties or an increase in activity due to higher expression levels on the surface of the yeast cells. These tended to be found more distant from the catalytic site (avg. distance 29 Å; avg. distance all=17 Å).

To identify candidate hotspots for catalytic enhancement, we considered the range of neutral fitness scores found for the synonymous mutants (Expression fitness= -0.03±0.091; Activity fitness=-0.01±0.064, Fig. 2*F,H*). We found 148 (~2% of total) single mutant variants associated with neutral expression scores (-0.121 <Exp < 0.054) that exhibited activity fitness higher than the range given by synonymous mutations (Activity fitness >0.061). Among these variants, we identified the 8 most

repeated protein sites represented by on average >50 cells in the activity dataset, and we mapped positions onto the 3D structure of DAOx (Fig. 5*B*). All the positions identified are located far from the catalytic site (min. distance= 10.7Å, max. distance =40.3Å, median distance =28.3 Å). Additionally, three sites were identified at the dimer interface (P45, P309, S311, avg. distance to interface = 0 Å) or on the flexible loop between beta β strands 12 and 13 (A319, A320) involved in homo dimerization of the enzyme[33,52]. These results suggest that mutations at these positions can improve catalysis by stabilizing the quaternary dimer (which is necessary for catalysis), while not significantly influencing overall expression levels. Other sites included Glu98 located at the entrance of the substrate tunnel, which was the most frequently found mutational hotspot (n=7/29) associated with improvement in activity, suggesting a possible impact on the interactions with the D-Ala substrate. Finally, we can speculate that altering Asp170 located in the flexible loop between β strand 6 and α helix 7, or Ala296 found on the opposite side of the dimer interface might lead to conformational changes of the overall structure causing allosteric effects on the catalysis of the enzyme (Fig. 5B).

Conclusions

EP-Seq is a deep mutational scanning workflow for studying enzyme folding stability and catalytic activity. Yeast surface display combined with peroxidase-mediated proximity labeling of single cells was able to link enzymatic activity to fluorescent phenotypes for large libraries in a pooled format, enabling cell sorting and high-throughput sequencing. We demonstrated our workflow by constructing a near comprehensive single substitution variant library of DAOx, and assaying it by EP-Seq for folding stability and catalytic activity. By jointly analyzing the expression and activity fitness datasets as a function of various biophysical and biochemical properties of the mutated residues at WT residues, we gained structural and biophysical insight into DAOx.

When considering the correlation of fitness score with various biophysical parameters of the mutated residues, for many parameters the two datasets exhibited high concordance. This indicates that in order for a variant to be catalytically active, it must first be stably expressed and secreted to the cell wall. We therefore observed an expression level-dependency of the catalytic activity. However, our data further revealed certain properties of mutated sites which were differentially correlated with expression and activity fitness. These included distance of the mutated residue to the FAD cofactor and distance to the dimer interface. We found that WT residues in close proximity to the FAD cofactor in the active site tended to destabilize the enzyme, and could be mutated to enhance folding stability, however this stability was achieved at the cost of catalytic activity. This demonstrates functional constraints that have shaped the evolution of DAOx over time, and provides direct evidence of an activity-stability tradeoff. The distance of the mutated residues to the dimer interface was similarly decoupled between expression and activity fitness datasets. Prior literature[51,52] indicates dimerization is necessary but not sufficient for catalytic activity. Mutations that disrupted the dimer interface therefore functioned similarly to those in the active site, where destabilizing the dimer interface through mutation could lead to higher overall expression, however this increased stability was achieved at the cost of catalytic activity. Our workflow is compatible with studying enzymes that can be directly or indirectly (via enzymatic cascade) linked to the production of peroxide (Fig. S8). Due to its inherent scalability, our approach will find applications in generating training data for machine learning algorithms, which represents a major challenge for catalytic enzymes. In the future, EP-Seq can contribute to a better understanding of evolutionary processes in natural enzymes, help in

identifying functional allosteric sites, and be used to evolve protein catalysts for industrial and biomedical applications.

Acknowledgments

This work was supported by the University of Basel, ETH Zurich, the SNF-NCCR in Molecular Systems Engineering, and an SNSF Grant (200021_191962) to M.A.N. The authors thank the following individuals for helpful discussions: Joanan Lopez Morales, Jaime de Santaella, Olena Protsenko.

References

1. Currin, A., Swainston, N., Day, P. J. & Kell, D. B. Synthetic biology for the directed evolution of protein biocatalysts: navigating sequence space intelligently. *Chem. Soc. Rev.* **44**, 1172–1239 (2015).
2. Siddiqui, K. S. Defying the activity-stability trade-off in enzymes: taking advantage of entropy to enhance activity and thermostability. *Crit. Rev. Biotechnol.* **37**, 309–322 (2017).
3. Goldenzweig, A. & Fleishman, S. J. Principles of Protein Stability and Their Application in Computational Design. *Annu. Rev. Biochem.* **87**, 105–129 (2018).
4. Feller, G. Protein stability and enzyme activity at extreme biological temperatures. *J. Phys. Condens. Matter* **22**, 323101 (2010).
5. Arcus, V. L., van der Kamp, M. W., Pudney, C. R. & Mulholland, A. J. Enzyme evolution and the temperature dependence of enzyme catalysis. *Curr. Opin. Struct. Biol.* **65**, 96–101 (2020).
6. Akanuma, S. *et al.* Establishment of mesophilic-like catalytic properties in a thermophilic enzyme without affecting its thermal stability. *Sci. Rep.* **9**, (2019).
7. Stark, C., Bautista-Leung, T., Siegfried, J. & Herschlag, D. Systematic investigation of the link between enzyme catalysis and cold adaptation. *Elife* **11**, (2022).
8. Miller, S. R. An appraisal of the enzyme stability-activity trade-off. *Evolution* **71**, 1876–1887 (2017).
9. Zeymer, C. & Hilvert, D. Directed Evolution of Protein Catalysts. *Annu. Rev. Biochem.* (2018) doi:10.1146/annurev-biochem-062917-012034.
10. Rix, G. *et al.* Scalable continuous evolution for the generation of diverse enzyme variants encompassing promiscuous activities. *Nat. Commun.* **11**, 5644 (2020).
11. Araya, C. L. & Fowler, D. M. Deep mutational scanning: assessing protein function on a massive scale. *Trends Biotechnol.* **29**, 435–442 (2011).
12. Fowler, D. M. & Fields, S. Deep mutational scanning: a new style of protein science. *Nat. Methods* **11**, 801–807 (2014).

13. Vanella, R., Kovacevic, G., Doffini, V., de Santaella, J. F. & Nash, M. A. High-throughput screening, next generation sequencing and machine learning: advanced methods in enzyme engineering. *Chem. Commun.* **58**, 2455–2467 (2022).

14. Melnikov, A., Rogov, P., Wang, L., Gnirke, A. & Mikkelsen, T. S. Comprehensive mutational scanning of a kinase in vivo reveals substrate-dependent fitness landscapes. *Nucleic Acids Res.* **42**, e112 (2014).

15. Chen, J. Z., Fowler, D. M. & Tokuriki, N. Environmental selection and epistasis in an empirical phenotype-environment-fitness landscape. *Nat Ecol Evol* **6**, 427–438 (2022).

16. Wrenbeck, E. E., Azouz, L. R. & Whitehead, T. A. Single-mutation fitness landscapes for an enzyme on multiple substrates reveal specificity is globally encoded. *Nat. Commun.* **8**, 15695 (2017).

17. Stiffler, M. A., Hekstra, D. R. & Ranganathan, R. Evolvability as a function of purifying selection in TEM-1 β-lactamase. *Cell* **160**, 882–892 (2015).

18. Romero, P. A., Tran, T. M. & Abate, A. R. Dissecting enzyme function with microfluidic-based deep mutational scanning. *Proc. Natl. Acad. Sci. U. S. A.* **112**, 7159–7164 (2015).

19. Roychowdhury, H. & Romero, P. A. Microfluidic deep mutational scanning of the human executioner caspases reveals differences in structure and regulation. *Cell Death Discov* **8**, 7 (2022).

20. Debon, A. *et al.* Ultrahigh-throughput screening enables efficient single-round oxidase remodelling. *Nature Catalysis* **2**, 740–747 (2019).

21. Klesmith, J. R., Bacik, J.-P., Wrenbeck, E. E., Michalczyk, R. & Whitehead, T. A. Trade-offs between enzyme fitness and solubility illuminated by deep mutational scanning. *Proceedings of the National Academy of Sciences* **114**, 2265–2270 (2017).

22. Markin, C. J. *et al.* Revealing enzyme functional architecture via high-throughput microfluidic enzyme kinetics. *Science* **373**, (2021).

23. Boder, E. T. & Wittrup, K. D. Yeast surface display for screening combinatorial polypeptide

libraries. *Nat. Biotechnol.* **15**, 553–557 (1997).

24. Starr, T. N. *et al.* Deep Mutational Scanning of SARS-CoV-2 Receptor Binding Domain Reveals Constraints on Folding and ACE2 Binding. *Cell* **182**, 1295-1310.e20 (2020).
25. Lipovsek, D. *et al.* Selection of horseradish peroxidase variants with enhanced enantioselectivity by yeast surface display. *Chem. Biol.* **14**, 1176–1185 (2007).
26. Vanella, R., Bazin, A., Ta, D. T. & Nash, M. A. Genetically Encoded Stimuli-Responsive Cytoprotective Hydrogel Capsules for Single Cells Provide Novel Genotype–Phenotype Linkage. *Chem. Mater.* (2019) doi:10.1021/acs.chemmater.8b04348.
27. Vanella, R., Ta, D. T. & Nash, M. A. Enzyme-mediated hydrogel encapsulation of single cells for high-throughput screening and directed evolution of oxidoreductases. *Biotechnol. Bioeng.* (2019) doi:10.1002/bit.27002.
28. Rosini, E. *et al.* An antibody-based enzymatic therapy for cancer treatment: The selective localization of D-amino acid oxidase to EDA fibronectin. *Nanomedicine* 102424 (2021).
29. Rosini, E., Pollegioni, L., Ghisla, S. & Orru, R. Optimization of d-amino acid oxidase for low substrate concentrations–towards a cancer enzyme therapy. *FEBS J.* (2009).
30. Pollegioni, L. & Molla, G. New biotech applications from evolved D-amino acid oxidases. *Trends Biotechnol.* **29**, 276–283 (2011).
31. Li, J., Shen, Y., Liu, A., Wang, X. & Zhao, C. Transfection of the DAAO gene and subsequent induction of cytotoxic oxidative stress by D-alanine in 9L cells. *Oncol. Rep.* **20**, 341–346 (2008).
32. Khoronenkova, S. V. & Tishkov, V. I. D-amino acid oxidase: physiological role and applications. *Biochemistry* **73**, 1511–1518 (2008).
33. Pollegioni, L. *et al.* Yeast D-amino acid oxidase: structural basis of its catalytic properties. *J. Mol. Biol.* **324**, 535–546 (2002).
34. Ellgaard, L. & Helenius, A. Quality control in the endoplasmic reticulum. *Nat. Rev. Mol. Cell Biol.* **4**, 181–191 (2003).
35. Li, X.-W. *et al.* New insights into the DT40 B cell receptor cluster using a proteomic proximity

labeling assay. *J. Biol. Chem.* **289**, 14434–14447 (2014).

36. Singer-Krüger, B. *et al.* APEX2-mediated proximity labeling resolves protein networks in Saccharomyces cerevisiae cells. *FEBS J.* **287**, 325–344 (2020).
37. Kim, D. I. & Roux, K. J. Filling the Void: Proximity-Based Labeling of Proteins in Living Cells. *Trends Cell Biol.* **26**, 804–817 (2016).
38. Honke, K. & Kotani, N. Identification of cell-surface molecular interactions under living conditions by using the enzyme-mediated activation of radical sources (EMARS) method. *Sensors* **12**, 16037–16045 (2012).
39. Kotani, N. *et al.* Biochemical visualization of cell surface molecular clustering in living cells. *Proc. Natl. Acad. Sci. U. S. A.* **105**, 7405–7409 (2008).
40. Lam, S. S. *et al.* Directed evolution of APEX2 for electron microscopy and proximity labeling. *Nat. Methods* **12**, 51–54 (2015).
41. Hopkins, C., Gibson, A., Stinchcombe, J. & Futter, C. Chimeric molecules employing horseradish peroxidase as reporter enzyme for protein localization in the electron microscope. *Methods Enzymol.* **327**, 35–45 (2000).
42. van Gijlswijk, R. P. *et al.* Fluorochrome-labeled tyramides: use in immunocytochemistry and fluorescence in situ hybridization. *J. Histochem. Cytochem.* **45**, 375–382 (1997).
43. Hunyady, B., Krempels, K., Harta, G. & Mezey, E. Immunohistochemical signal amplification by catalyzed reporter deposition and its application in double immunostaining. *J. Histochem. Cytochem.* **44**, 1353–1362 (1996).
44. Rosini, E. PEG-DAAO conjugate: A promising tool for cancer therapy optimized by protein engineering. *Nanomedicine* 102122 (2019).
45. Malinowska, K. H. & Nash, M. A. Enzyme- and affinity biomolecule-mediated polymerization systems for biological signal amplification and cell screening. *Curr. Opin. Biotechnol.* **39**, 68–75 (2016).
46. Agresti, J. J. *et al.* Ultrahigh-throughput screening in drop-based microfluidics for directed

evolution. *Proc. Natl. Acad. Sci. U. S. A.* **107**, 4004–4009 (2010).

47. Schymkowitz, J. *et al.* The FoldX web server: an online force field. *Nucleic Acids Res.* **33**, W382-8 (2005).
48. Chung-Jung Tsai, Buyong Ma, and Ruth Nussinov. Intra-molecular chaperone: the role of the N-terminal in conformational selection and kinetic control. *Physical Biology* **6**, (2009).
49. Gasteiger, E. *et al.* Protein Identification and Analysis Tools on the ExPASy Server. in *The Proteomics Protocols Handbook* (ed. Walker, J. M.) 571–607 (Humana Press, 2005).
50. Pollegioni, L., Piubelli, L., Sacchi, S., Pilone, M. S. & Molla, G. Physiological functions of D-amino acid oxidases: from yeast to humans. *Cell. Mol. Life Sci.* **64**, 1373–1394 (2007).
51. Casalin, P., Pollegioni, L., Curti, B. & Pilone Simonetta, M. A study on apoenzyme from Rhodotorula gracilis D-amino acid oxidase. *Eur. J. Biochem.* **197**, 513–517 (1991).
52. Piubelli, L., Caldinelli, L., Molla, G., Pilone, M. S. & Pollegioni, L. Conversion of the dimeric D-amino acid oxidase from Rhodotorula gracilis to a monomeric form. A rational mutagenesis approach. *FEBS Lett.* **526**, 43–48 (2002).
53. Cagiada, M. *et al.* Discovering functionally important sites in proteins. *bioRxiv* 2022.07.14.500015 (2022) doi:10.1101/2022.07.14.500015.
54. Cagiada, M. *et al.* Understanding the Origins of Loss of Protein Function by Analyzing the Effects of Thousands of Variants on Activity and Abundance. *Mol. Biol. Evol.* **38**, 3235–3246 (2021).
55. Caldinelli, L., Molla, G., Pilone, M. S. & Pollegioni, L. Tryptophan 243 affects interprotein contacts, cofactor binding and stability in D-amino acid oxidase from Rhodotorula gracilis. *FEBS J.* **273**, 504–512 (2006).
56. Gustavsson, M. *et al.* Stable linker peptides for a cellulose-binding domain-lipase fusion protein expressed in Pichia pastoris. *Protein Eng.* **14**, 711–715 (2001).
57. Gietz, R. D. & Woods, R. A. Transformation of yeast by lithium acetate/single-stranded carrier DNA/polyethylene glycol method. *Methods Enzymol.* **350**, 87–96 (2002).
58. Wrenbeck, E. E. *et al.* Plasmid-based one-pot saturation mutagenesis. *Nat. Methods* **13**, 928–

930 (2016).

59. Bloom, J. D. An experimentally determined evolutionary model dramatically improves phylogenetic fit. *Mol. Biol. Evol.* **31**, 1956–1978 (2014).

60. Li, H. Minimap2: pairwise alignment for nucleotide sequences. *Bioinformatics* **34**, 3094–3100 (2018).

61. Bushnell, B. BBMap: A Fast, Accurate, Splice-Aware Aligner. *https://www.semanticscholar.org › paper › BBMap:-A-Fas...https://www.semanticscholar.org › paper › BBMap:-A-Fas...* (2014).

62. Robert, X. & Gouet, P. Deciphering key features in protein structures with the new ENDscript server. *Nucleic Acids Res.* **42**, W320-4 (2014).

63. Sacchi, S. *et al.* Engineering the substrate specificity of D-amino-acid oxidase. *J. Biol. Chem.* **277**, 27510–27516 (2002).

64. Becker, S. *et al.* Single-cell high-throughput screening to identify enantioselective hydrolytic enzymes. *Angew. Chem. Int. Ed Engl.* **47**, 5085–5088 (2008).

65. Ostafe, R., Prodanovic, R., Nazor, J. & Fischer, R. Ultra-high-throughput screening method for the directed evolution of glucose oxidase. *Chem. Biol.* **21**, 414–421 (2014).

66. Imai, K. & Mitaku, S. Mechanisms of secondary structure breakers in soluble proteins. *Biophysics* **1**, 55–65 (2005).

67. Gray, V. E., Hause, R. J. & Fowler, D. M. Analysis of Large-Scale Mutagenesis Data To Assess the Impact of Single Amino Acid Substitutions. *Genetics* **207**, 53–61 (2017).